Geophysical Research Letters

RESEARCH LETTER
10.1029/2021GL097574

Special Section:
Southern Ocean and Climate: Biogeochemical and Physical Fluxes and Processes

Enhanced Ventilation in Energetic Regions of the Antarctic Circumpolar Current

Lilian A. Dove[1], Dhruv Balwada[2], Andrew F. Thompson[1], and Alison R. Gray[3]

[1]Division of Geological and Planetary Sciences, Environmental Science and Engineering, California Institute of Technology, Pasadena, CA, USA, [2]Lamont-Doherty Earth Observatory, Columbia University, Palisades, NY, USA, [3]School of Oceanography, University of Washington, Seattle, WA, USA

Key Points:

- The relationship between apparent oxygen utilization (AOU) and eddy kinetic energy (EKE) is assessed in the Antarctic Circumpolar Current
- AOU has relatively reduced values below the mixed layer in high-EKE standing meanders as compared to low-EKE regions
- Modification of the density structure and enhanced meso- and submesoscale motions enhance ventilation in standing meanders

Supporting Information:

Supporting Information may be found in the online version of this article.

Correspondence to:

L. A. Dove,
dove@caltech.edu

Citation:

Dove, L. A., Balwada, D., Thompson, A. F., & Gray, A. R. (2022). Enhanced ventilation in energetic regions of the Antarctic Circumpolar Current. *Geophysical Research Letters*, *49*, e2021GL097574. https://doi.org/10.1029/2021GL097574

Received 22 DEC 2021
Accepted 16 JUN 2022

Abstract Flow-topography interactions along the path of the Antarctic Circumpolar Current generate standing meanders, create regions of enhanced eddy kinetic energy (EKE), and modify frontal structure. We consider the impact of standing meanders on ventilation based on oxygen measurements from Argo floats and the patterns of apparent oxygen utilization (AOU). Regions of high-EKE have relatively reduced AOU values at depths 200–700 m below the base of the mixed layer and larger AOU variance, suggesting enhanced ventilation due to both along-isopycnal stirring and enhanced exchange across the base of the mixed layer. Vertical exchange is inferred from finite-size Lyapunov exponents, a proxy for the magnitude of surface lateral density gradients, which suggest that submesoscale vertical velocities may contribute to ventilation. The shaping of ventilation by standing meanders has implications for the temporal and spatial variability of air–sea exchange.

Plain Language Summary The circulation of the Southern Ocean is dominated by the eastward-flowing Antarctic Circumpolar Current (ACC). The characteristics of the ACC are not uniform around the Southern Ocean. Rather, when the ACC encounters underwater mountain ranges the flow is diverted, which causes these regions to be more energetic through the generation of ocean eddies in a process similar to atmospheric storm tracks. Numerical models have suggested that the exchange of properties, such as heat and carbon dioxide, between the atmosphere and the interior ocean is enhanced in these energetic regions. In this study, data from freely floating robotic floats in the Southern Ocean is used to observe the vertical structure of dissolved oxygen. Transfer of properties between the ocean's surface and the interior ocean preferentially occurs in high energy regions of the ACC. Most previous work has relied on numerical models of the ocean that, due to computational limits, do not represent all aspects of the ACC's energetic regions. This study has implications for how the Southern Ocean's ability to take up excess carbon dioxide from the atmosphere will evolve in the future.

1. Introduction

The Southern Ocean is a key region for the ventilation and formation of intermediate and deep water masses. Tilted density surfaces associated with the Antarctic Circumpolar Current (ACC) allow for the adiabatic upwelling of Circumpolar Deep Water (CDW) that has been sequestered from the surface for O(100–1000 years). At the surface, CDW exchanges heat and gases with the atmosphere, outgassing natural carbon stocks and acting as a sink for anthropogenic CO_2 (Gruber et al., 2019; Landschützer et al., 2015). Numerical models suggest that ventilation is spatially heterogeneous within the ACC (Tamsitt et al., 2017; Viglione & Thompson, 2016). Interactions of the ACC with underwater topography can result in the diversion and compaction of frontal currents, creating standing meanders (Sokolov & Rintoul, 2007) associated with enhanced mesoscale eddy kinetic energy (EKE; Figures 1a and 1b) (Gille & Kelly, 1996). The ACC's major standing meanders are present at the Kergeulen Plateau, Campbell Plateau, Eastern Pacific Rise, Crozet Plateau, and Drake Passage; these regions are thought to shape uptake and sequestration of heat and carbon (Brady et al., 2021; Klocker, 2018; Roach et al., 2016; Sallée et al., 2012).

Ventilation in the ACC depends on the local density structure as well as advection and stirring along isopycnals, and thus responds to a variety of processes and scales. Standing meanders lead to sloped isopycnals that store available potential energy (Bischoff & Thompson, 2014; Chapman et al., 2015; Klocker, 2018), which is released by baroclinic instability, producing a rich mesoscale O(100 km) eddy field approximately 100 km downstream of the standing meander (Rintoul, 2018; Thompson & Naveira Garabato, 2014). These eddies then stir

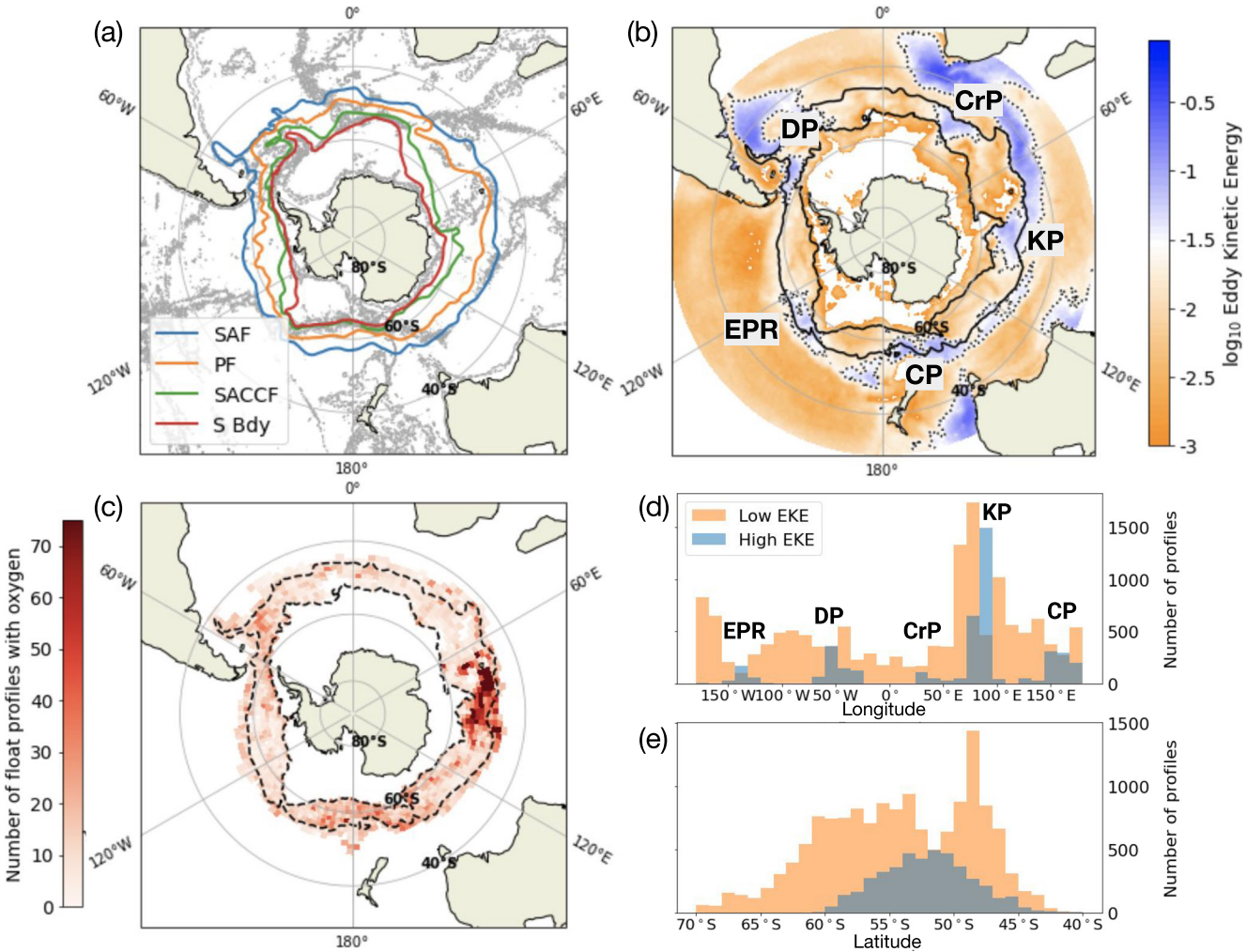

Figure 1. (a) Bathymetry and major fronts of the Southern Ocean. Gray contours show 1,000, 2,000, and 3,000 m isobaths. Fronts are the Subantarctic Front (blue), Polar Front (orange), Southern Antarctic Circumpolar Current Front (green), and the Southern Boundary (red). (b) Base-10 logarithm of eddy kinetic energy (EKE) [$\log_{10}$ m^2 s^{-2}]. Black solid lines show the Antarctic Circumpolar Current (ACC) boundaries used in this study. Black dotted lines denote regions of high EKE. Standing meanders are labeled by the corresponding bathymetric feature: Crozet Plateau (CrP), Kerguelen Plateau (KP), Campbell Plateau (CP), East Pacific Rise (EPR), and Drake Passage (DP). (c) Spatial distribution of float profiles containing oxygen data across the Southern Ocean within the ACC; Δlatitude = 1.25°, Δlongitude = 2.5°. Black dotted lines show the ACC boundaries used in this study. (d) Histogram of the number of float profiles as a function of longitude within the ACC boundaries in panel (b). Profiles categorized as low-EKE are in orange, with high-EKE profiles in blue. Standing meanders are labeled the same as in panel (b). (e) Histogram of the number of float profiles at a given latitude within the ACC boundaries in panel (b). Colors are the same as in panel (d).

and strain the surface density field, leading to frontogenesis and influencing submesoscale motions (Bachman & Klocker, 2020; Balwada et al., 2018; Klein & Lapeyre, 2009; Rosso et al., 2015). Through both lateral (Abernathey & Marshall, 2013; Roach et al., 2018) and vertical (Adams et al., 2017; Klein & Lapeyre, 2009) motions, mesoscale and submesoscale eddies contribute significantly to ventilation in the ACC. Throughout this work, we refer to "ventilation" as any process or combination of processes that work to transfer surface waters and tracers into the pycnocline, which as described above, can occur on a variety of temporal and spatial scales (Morrison et al., 2022). Additionally, stirring refers to the advection of tracers by an eddying velocity field, while mixing is an irreversible process that removes tracer variance; only the former contributes directly to ventilation although mixing influences the interpretation of ventilation from tracer distributions (Villermaux, 2019).

Numerical models demonstrate that regions with higher EKE have enhanced capacity for submesoscale transport of tracers across the base of the mixed layer (Balwada et al., 2018; Lévy et al., 2018; Uchida et al., 2020) and can have an outsized impact on ventilation (Naveira Garabato et al., 2011; Rintoul, 2018; Tamsitt et al., 2016; Viglione & Thompson, 2016). Standing meanders have also been identified as regions where older waters

enriched in dissolved inorganic carbon are preferentially transported to the surface (Brady et al., 2021; Tamsitt et al., 2017), which can potentially create local regions of enhanced air–sea gas exchange. Observational studies are needed to validate these largely numerical results.

Due to coarse, ship-based sampling, examination of spatial variations in ventilation has focused on the basin (or ACC sector) scale (Morrison et al., 2022; Sallée et al., 2012). More recently, observations from floats have shown that air–sea fluxes of carbon (Gray et al., 2018) and oxygen (Bushinsky et al., 2017) vary across the Southern Ocean. Evidence for finer-scale variability in biogeochemical distributions comes from the analysis of Biogeochemical Argo (BGC-Argo) profiles, in which subsurface tracer anomalies are found to be more prevalent in high-EKE regions, suggesting stronger ventilation and export (Llort et al., 2018). High-resolution glider observations near the Southwest Indian Ridge also showed reduced vertical tracer gradients in the standing meander as compared to the low-EKE region downstream (Dove et al., 2021). Although these observational studies have provided initial evidence for the importance of standing meanders in ventilation, the physical processes in the ACC that set the dominant spatial and temporal scales of variability in surface-interior exchange have not yet been fully explored.

This study uses the broad spatial coverage of subsurface dissolved oxygen measurements collected by the BGC-Argo array, as well as remote sensing products, to consider controls on apparent oxygen utilization (AOU) patterns in the Southern Ocean and its relationship to ventilation of surface waters. Both vertical and isopycnal distributions of AOU exhibit substantial variations along the path of the ACC that can be linked primarily to enhanced ventilation in the ACC's major standing meanders. We identify several physical mechanisms that are consistent with these distributions. This work is a critical step for validating ocean models and observationally describing key regions of ventilation of climatologically important tracers in the Southern Ocean.

2. Data and Methods

2.1. Biogeochemical-Argo Floats

The Argo program has deployed over 10,000 profiling floats across the global ocean since 1999 (Riser et al., 2016) with the Southern Ocean Carbon and Climate Observations and Modeling (SOCCOM) program playing a vital role in increasing the BGC-Argo population of the Southern Ocean (Claustre et al., 2020; Johnson et al., 2017). Argo floats sample the upper 2,000 m of the ocean every 10 days. In between profiles, the floats drift at 1,000 m and follow a quasi-Lagrangian trajectory (Roemmich et al., 2009).

This study uses 21,941 profiles of dissolved oxygen, along with the associated temperature and salinity profiles, that were collected within the boundaries of the ACC (defined in Section 2.3) during the period 15 January 2003–16 May 2021 (Figures 1c–1e). Only data that have undergone delayed-mode quality control procedures and have been flagged as "good" are used in this analysis. All profile data were obtained from the "Sprof" files provided by the Argo Global Data Assembly Center, which merge biogeochemical samples that are measured at slightly different vertical positions onto a single common pressure axis.

2.2. Derived Variables

AOU is the difference between oxygen saturation concentration and observed dissolved oxygen concentrations ($AOU = O_2^{sat.} - O_2^{obs.}$), where the oxygen saturation is a function of the observed conservative temperature and absolute salinity. AOU in the surface ocean is typically close to 0 due to equilibration with the atmosphere. Bushinsky et al. (2017) showed that $AOU \approx 0$ is generally true for the ACC, but small variations of $\pm$5–10 μmol kg^{-1} exist due to biological activity, surface heat fluxes, or rapid entrainment of thermocline waters (Ito et al., 2004). Lower AOU values are used as a proxy for younger age, signaling recent ventilation, since respiration in the ocean interior is a persistent oxygen sink. AOU is a non-conservative tracer with its value determined by several processes, for example, remineralization, along-isopycnal stirring, cross-isopycnal mixing, and the non-conservative nature of solubility. AOU has been used to trace pathways between the surface and interior (Llort et al., 2018), and both vertical and along-isopycnal variations provide insight into ventilation dynamics.

We study the distribution of AOU in both density and depth coordinates. Additionally, to account for temporal and spatial variations in mixed layer depths (MLDs), vertical variations in AOU are also considered as deviations from the observed values at the base of the mixed layer in each profile. Depth below the base of the mixed layer

is given by Δh, and ΔAOU refers to the difference in AOU between the value at Δh and at the MLD. The MLD was defined by a density difference criterion of 0.03 kg m^{-3} from the surface (de Boyer Montégut et al., 2004). Other derived variables, such as potential density, were calculated from temperature and salinity using the Thermodynamic Equation of Seawater 2010 (McDougall & Barker, 2011).

2.3. Satellite Data

EKE was calculated as $\mathrm{EKE} = \frac{1}{2}\sqrt{\overline{u'^2} + \overline{v'^2}}$, where u' and v' are the zonal and meridional eddy geostrophic velocities estimated from the time-varying sea surface height anomaly field, and $\overline{(.)}$ represents a time average calculated over 1993–2016. Regions with EKE greater than 250 $cm^2\ s^{-2}$ were considered "high-EKE" (Figures 1b and S1 in Supporting Information S1), and individual float profiles were tagged as "high" or "low" EKE based on their surfacing locations. Previous studies have identified distinct dynamical regimes within individual standing meanders (Barthel et al., 2017; Youngs et al., 2017), but we do not distinguish these here.

The ACC boundaries were defined using absolute dynamic topography (ADT) with the northern and southern boundaries given by the −0.1 m and the −1.05 m ADT contours, respectively. These boundaries were selected in part to avoid inclusion of the Agulhas Retroflection, which is a region of enhanced EKE but is not considered in this study. Several definitions of the northern and southern boundaries of the ACC were tested, including hydrographic definitions of frontal boundaries (shown in Figure 1a) as opposed to sea level anomaly (Kim & Orsi, 2014), but these led to minimal differences in the results.

Finite-size Lyapunov Exponents (FSLEs) describe the orientation and timescale of strain fields by quantifying stretching and compression (d'Ovidio et al., 2004, 2010). They are a Lagrangian diagnostic, and for a given flow field are defined as the separation growth rate for particle pairs, $\lambda(d_0, d_f) = \frac{1}{\tau}\log\left(\frac{d_f}{d_0}\right)$, where d_0 and d_f are the initial and final separation distances and τ is the first time where the separation distance d_f is reached. Here we use FSLE estimates provided by AVISO+ that were computed from satellite-derived geostrophic velocities. We use the FSLEs from 1 January 2018 to 31 December 2020, but the exact choice of the period does not impact the results.

3. Results

3.1. Subsurface Signatures of Ventilation

Variations in AOU with depth and density may arise from various mechanisms, some reflecting differences in advection and stirring at scales smaller than the standing meander (discussed in Section 3.2), and others related to the larger-scale density structure of the ACC. A simple partitioning of individual float profiles between high- and low-EKE regions reveals striking differences in the vertical structure of AOU between these two regimes (Figure 2). Just below the mixed layer, for example, Δh = 100 m, high- and low-EKE regions both have low ΔAOU values with similar distributions (Figure 2a), although low-EKE regions have a longer tail. At Δh = 300 m, high- and low-EKE regions have distinct peaks with the high-EKE region having a lower median; the difference in the distributions' medians is 27 μmol kg^{-1} and the difference in the modes is 68 μmol kg^{-1} (Figures 2b and 2d). For values of Δh ≥ 700 m, the two regions have approximately the same distribution, with a difference in medians of only 2 μmol kg^{-1} (Figures 2c and 2d). The largest disparity in ΔAOU between the high- and low-EKE regions is present for 200 < Δh < 700 m (Figure 2d). This ΔAOU structure is set, in part, by meanders of the ACC that horizontally transport lighter waters southward into energetic regions downstream of topography. At the level of individual standing meanders, the high-EKE regions associated with the Kerguelen Plateau, Campbell Plateau, and Eastern Pacific Rise have distributions of ΔAOU that most closely align with the median distributions for the entire ACC (Figures 2fiii–2fv). The distinction between high- and low-EKE regions is weakest at the Crozet Plateau (Figure 2fii), although data availability is reduced here.

Changes in hydrographic properties along the path of the ACC provide insight into the origin of subsurface low-AOU waters found in high-EKE regions. CDW is distinguished by high salinity (>34.6 g kg^{-1}) and low temperature (~2°C). Comparatively, Antarctic Intermediate Water (AAIW), a more recently ventilated water mass, is characterized by lower salinity as a result of sea ice melt. Differences in hydrographic properties are

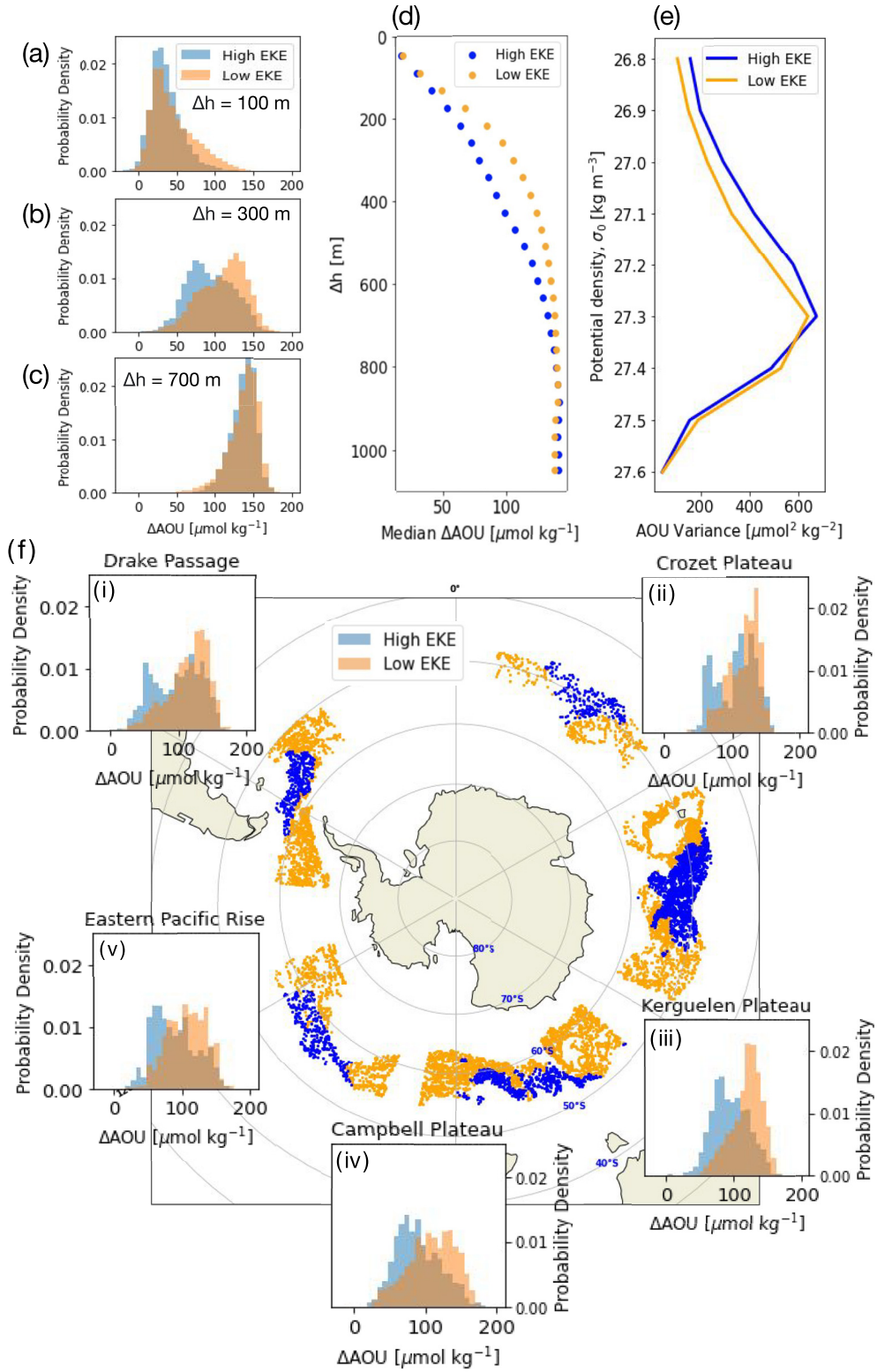

Figure 2. Probability density functions across the full Antarctic Circumpolar Current of ΔAOU [μmol kg^{-1}] where (a) Δh = 100 m, (b) Δh = 400 m, (c) Δh = 700 m. (d) Median in ΔAOU [μmol kg^{-1}] at values of Δh. (e) Variance of AOU [μmol^2 kg^{-2}] on potential density surfaces. (f) Locations of profiles used to create probability density functions of ΔAOU [μmol kg^{-1}] at Δh = 300 m at (i) Drake Passage, (ii) Crozet Plateau, (iii) Kerguelen Plateau, (iv) Campbell Plateau, and (v) Eastern Pacific Rise. In all panels, blue colors denote high-eddy kinetic energy (EKE) regions and orange colors denote low-EKE regions.

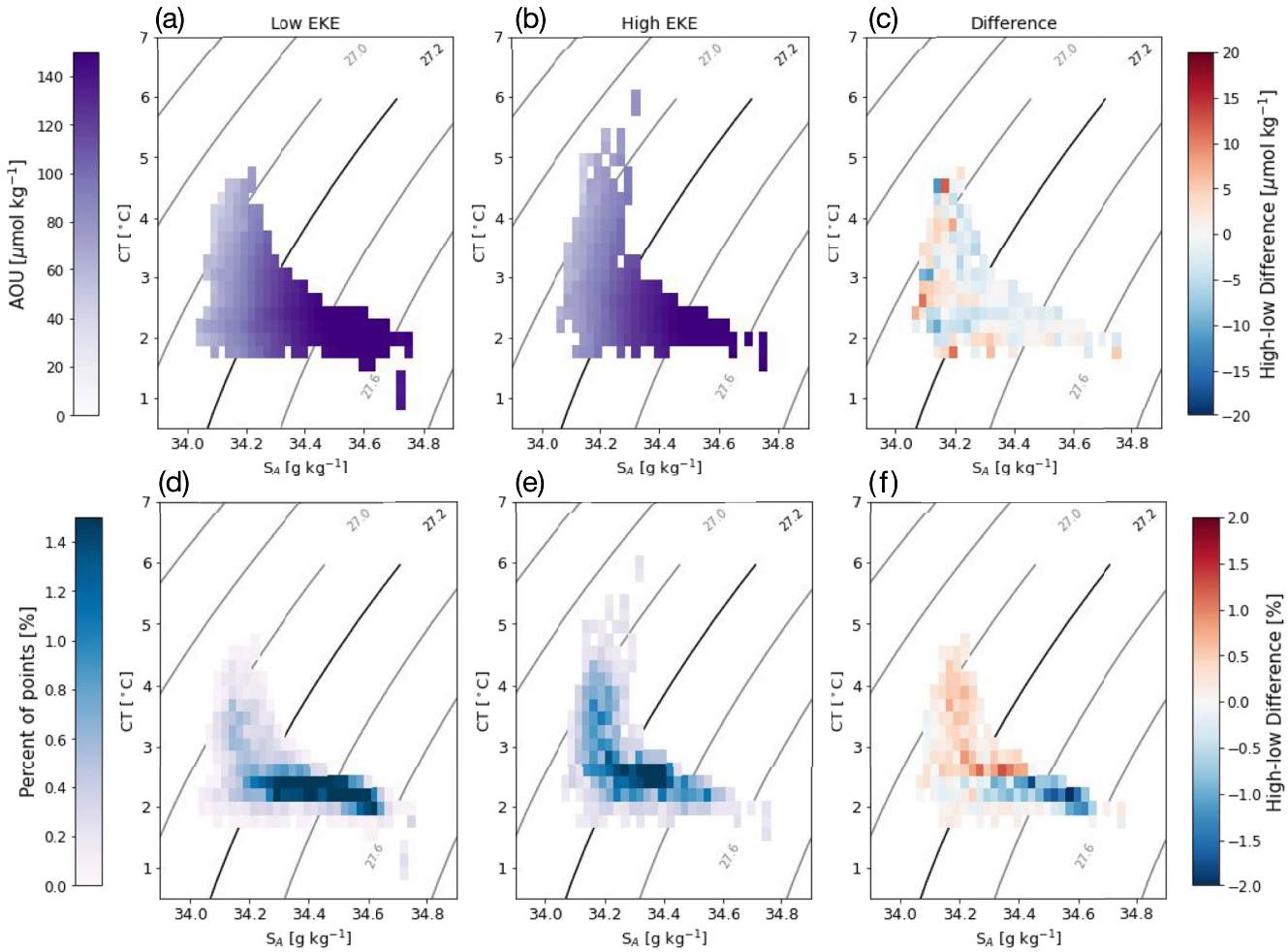

Figure 3. Absolute salinity (S_A)-conservative temperature (CT) diagrams. Average apparent oxygen utilization (AOU) for each S_A-CT position at $\Delta h = 300$ m in (a) the low-eddy kinetic energy (EKE) regions and (b) the high-EKE regions. (c) Difference in AOU between the low- and high-EKE regions. Joint histogram of profile locations at at $\Delta h = 300$ m in (d) the low-EKE regions, and (e) the high-EKE regions. (f) Difference in joint histograms between the low- and high-EKE regions. Gray contours are potential density [kg m^{-3}], with the black contour at 27.2 kg m^{-3}. In all panels, only where there were more than five points at a given CT-S_A value that could be averaged are shown. $\Delta CT = 0.2°C$, $\Delta S_A = 0.025$ g kg^{-1}.

particularly distinct around $\Delta h = 300$ m, consistent with large differences in ΔAOU medians between the high- and low-EKE regions (Figure 3). In both the high- and low-EKE regions at $\Delta h = 300$ m, the distributions of mean AOU as a function of temperature and salinity are similar (Figures 3a–3c), suggesting that ΔAOU is predominantly tied to the relative contributions of water masses below the mixed layer, with variations due to biology secondary. Stronger differences between the two regions are found, however, when considering the frequency distribution in conservative temperature-absolute salinity space (Figures 3d–3f). In the low-EKE regions, CDW properties dominate, with a temperature of 2°C and high salinity (34.4–34.8 g kg^{-1}; Figure 3d). In the high-EKE regions a greater fraction of the observations have lower values of salinity (34.0–34.2 g kg^{-1}) and also warmer temperatures (3–5°C; Figures 3e and 3f), consistent with intermediate waters that have been subducted from the surface. The increased presence of waters consistent with AAIW at these depths in the high-EKE regions suggests that more intermediate water is subducted in high-EKE regions of the ACC as compared to low-EKE regions.

This hydrographic analysis indicates that mixing of old CDW and recently ventilated AAIW at the basin-scale contributes to the patterns in ΔAOU described in Figure 2. Yet, coupled processes on the submesoscale–mesoscale spectrum may still play a role in setting these subsurface ΔAOU distributions, as described in previous observational work in standing meanders (Dove et al., 2021). Using an oxygen utilization rate (OUR) for the upper mesopelagic zone of 40 μmol kg^{-1} year^{-1} (Hennon et al., 2016), low ΔAOU waters with a median of O(70 μmol

kg^{-1}) in high-EKE regions would have an age of ~2 years, suggesting there may be recent injection from the mixed layer. However, estimates of OUR in the Southern Ocean are sparse and there is a good deal of uncertainty in the estimate of this time scale. Specifically, an OUR of 40 μmol kg^{-1} $year^{-1}$ represents a regional, near-surface value that may not be representative of values at greater depths or over the broader Southern Ocean. Therefore this OUR value should be considered an upper bound, and the low ΔAOU waters observed in high-EKE regions likely include waters that have been subducted below the surface boundary layer for periods longer than 2 years.

It is important to also consider AOU variations on density surfaces because the mean density structure between the high- and low-EKE regions is different: the lower EKE regions host denser isopycnals linked to deeper depths and higher AOU values in the mid- and low-latitude basins to the north (Figures S2a and S2b in Supporting Information S1). These variations along the path of the ACC are related to changes in outcropping density classes as well as the steepening of lateral density gradients within standing meanders (Chapman et al., 2015; Thompson & Naveira Garabato, 2014), which may enable recently ventilated surface waters to be displaced downward in the water column. Despite the different density ranges between the regions, the vertical stratification, measured by the vertical buoyancy gradient N^2, is similar (Figure S2c in Supporting Information S1). Considering the Argo observations in density space show that the heavier isopycnals have relatively homogeneous mean AOU distributions along the path of the ACC, which is likely a result of the rapid along-ACC circulation (Figures S3 and S4 in Supporting Information S1). However, lighter isopycnals and regions where isopycnals are shallower show inhomogeneities in mean AOU along the path of the ACC, due in part to the outcropping of denser isopycnals in low-EKE regions. Some of the signal of lower mean AOU concentrations, particularly at deeper depths, may be attributed to adiabatic heaving rather than ventilation by advection and mixing. In the next section, we offer evidence that high-EKE regions are subject to more energetic stirring, leading to enhanced along-isopycnal variance of AOU, suggesting that AOU variations do not result from isopycnal heaving alone.

3.2. Mesoscale and Submesoscale Contributions to Ventilation

Variations in AOU due to the ACC's density structure occur at standing meander and larger scales (≥1,000 km); below these scales, mesoscale and submesoscale motions can impact ventilation through a number of different mechanisms. These include (a) increased along-isopycnal stirring as a result of enhanced EKE; (b) frontal subduction as a result of frontogenesis in the standing meander; and (c) enhanced vertical transport by submesoscale motions. Here, we investigate how these processes shape along-ACC differences in AOU distributions.

Differences in isopycnal AOU variance between high- and low-EKE regions offers insight into how along-isopycnal stirring contributes to ventilation within the ACC. To remove the effects of vertical isopycnal displacement (i.e., heave; Figure S3 in Supporting Information S1), we consider deviations from a longitude-dependent (10-degree longitude bins), along-isopycnal mean AOU value. The variance in AOU on density surfaces <27.4 is up to 18% larger in high-EKE regions than in low-EKE regions, with a peak in variance at 27.3 kg m^{-3} in both regions. The observed enhanced AOU variance in high-EKE regions is consistent with along-isopycnal stirring bringing low-ΔAOU waters to depth, as opposed to this signal solely occurring due to variations in the ACC's large-scale density structure. Enhanced variance in the high-EKE regions may arise from both stirring processes and injection of tracer anomalies from the surface layer onto density surfaces below the mixed layer. With regard to exchange out of the mixed layer, seasonal or along-stream changes in mixed layer properties may be expected to modify ventilation. However, the float data indiciate that MLD and stratification at the base of the mixed layer are similar in high- and low-EKE regions and therefore do not contribute to the disparity in subsurface ΔAOU distributions (Figure S5 in Supporting Information S1).

In addition to being regions of energetic mesoscale eddies, ACC standing meanders are regions of strong surface frontogenesis that give rise to large mixed layer lateral density gradients. These gradients are reservoirs of potential energy that can give rise to instabilities that lead to intense submesoscale vertical motions and increase the efficiency of tracer transport between the surface and interior ocean, contributing to ventilation (Klein & Lapeyre, 2009; Lévy et al., 2018; Mahadevan, 2016). While these instabilities typically occur on spatial and temporal scales consistent with the submesoscale, they are shaped by the mesoscale flow field (Balwada et al., 2018, 2020; Rosso et al., 2015). We investigate the potential of enhanced ventilation occurring via frontogenesis and submesoscale subduction by considering the relative magnitude of lateral density gradients between low- and high-EKE regions. Measuring lateral density gradients can be achieved with high temporal and spatial resolution measurements, but such observations are sparse in the Southern Ocean. Siegelman et al. (2020)

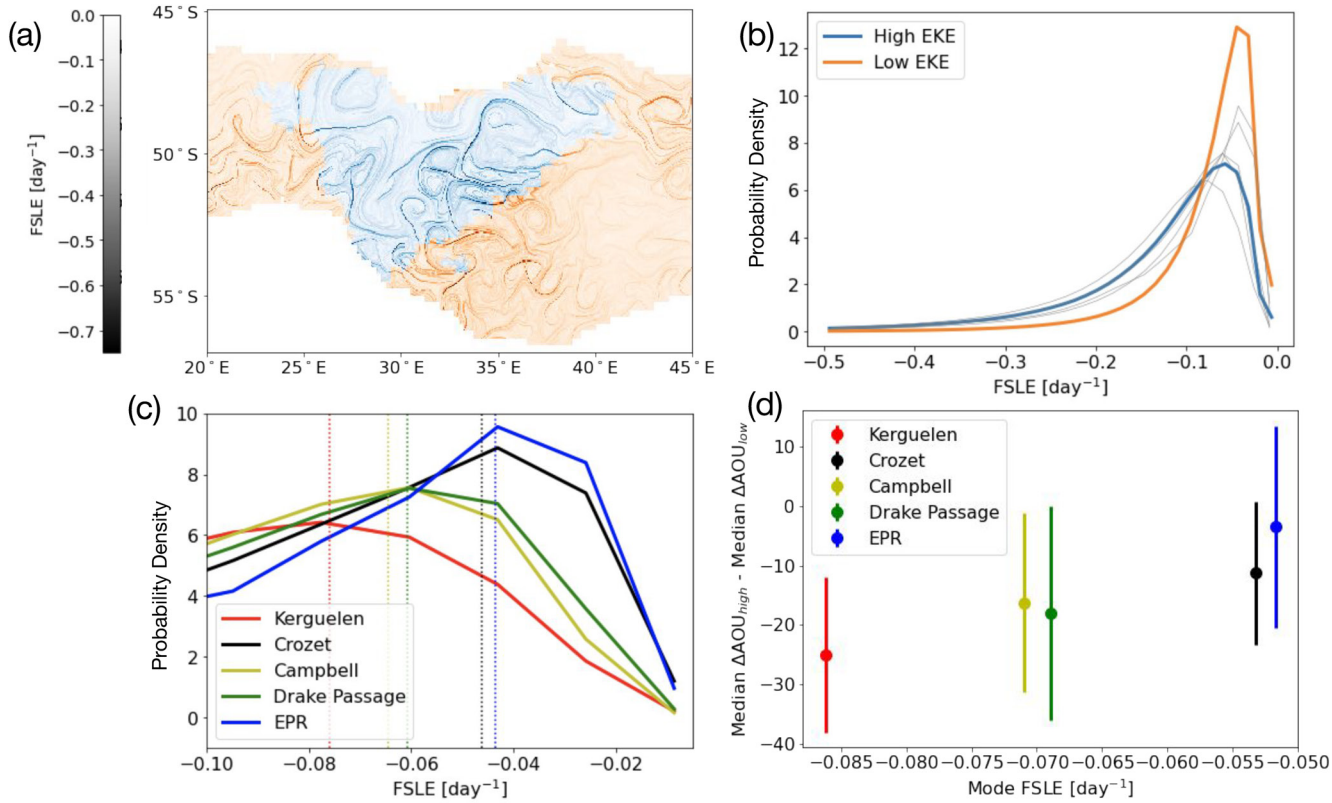

Figure 4. (a) Snapshot of Finite-size Lyapunov Exponents (FSLEs) from 1 March 2020 centered on the Crozet Plateau region of the Antarctic Circumpolar Current (ACC). Blue regions are high-eddy kinetic energy (EKE) while orange are low-EKE, using the EKE definition defined in the methods. (b) Probability density function of maximum stretching FSLE in the high- (blue) and low- (orange) EKE regions across the full ACC. Gray lines are expanded in panel (c). (c) Probability density function of maximum stretching FSLE in the Kergulen Plateau (red), the Crozet Plateau (black), the Campbell Plateau (yellow), Drake Passage (green), and the Eastern Pacific Rise (EPR; blue). Vertical lines represent 75th percentiles with the same colors as above. (d) Plot of the mode of the FSLE in the high-EKE region versus the differences in the high and low medians of the ΔAOU probability density functions (δAOU) at $\Delta h = 250$ m. Error bars are standard deviations of δAOU and colors are the same as in panel (c).

empirically showed that maximum stretching FSLEs (hereafter FSLEs) calculated from satellite-derived flow fields can be used to approximate the magnitude of lateral density gradients and derived a relationship between the two quantities. Specifically, density anomalies are physically aligned with FSLEs, so larger magnitude FSLEs are correlated with stronger lateral density gradients. While FSLEs have previously been linked to mixed-layer density gradients, Siegelman et al. (2020) demonstrated that this relationship may extend below the mixed layer in the Southern Ocean, particularly in energetic regions.

Consistent with the heterogeneous distribution of EKE in the ACC, lateral density gradients (as inferred from FSLEs) undergo abrupt transitions in standing meander regions (Figure 4a). The probability distribution of FSLE has a log-normal distribution within both low- and high-EKE regions (Figure 4b). However, in the high-EKE region, the median value is shifted to larger magnitudes and the distribution has a longer tail, which we link to stronger and more frequent small-scale surface density gradients. The FSLE probability density function also differs for each individual standing meander (Figure 4c). The standing meander at the Kerguelen Plateau has the most negative (strongest) FSLE values, implying an increased frequency of strong lateral density gradients and potentially enhanced vertical transport. The standing meanders associated with the Crozet Plateau and Eastern Pacific Rise have the least negative (weakest) mode of FSLE probability, with the Campbell Plateau and Drake Passage falling between the extremes.

To consider the relationship between FSLEs and ΔAOU within individual standing meanders, we define localized low-EKE regions that surround each high-EKE standing meander, defined between the north-south ACC boundaries and extending 5 degrees of longitude to either side of the meander. For each of the five major standing meander regions, the median difference in ΔAOU between the high- and *localized* low-EKE regions at

$\Delta h = 250$ m is calculated; we refer to this as δAOU. A large magnitude of δAOU represents large differences in ΔAOU distributions between the high-EKE standing meander and the surrounding low-EKE region, while a negative δAOU indicates a greater volume of low-AOU water in the high-EKE region. In other words, a large, negative value of δAOU suggests that the high-EKE region experiences enhanced ventilation as a result of the stirring and submesoscale subduction processes described above, as compared to the surrounding low-EKE region. Differences in FSLE distributions between meanders are correlated with differences in δAOU (Figure 4d) for depths of Δh up to 500 m. The standing meander that has the largest FSLE mode magnitude (implying strongest stirring), Kerguelen Plateau, is associated with the largest δAOU. Standing meander regions with smaller magnitude FSLE modes, the Eastern Pacific Rise and Crozet Plateau, have δAOU values closer to zero. While five meanders dominate the high-EKE regions in the ACC, this analysis suggests that contributions of low ΔAOU waters to depth may be localized to only one or two intense standing meanders, Kerguelen and Campbell plateaus, indicating these standing meanders may play the dominant role in ventilation of the ACC.

4. Discussion

Ventilation of surface properties and tracers can arise from a combination of large-scale circulation features, for example, shaping of density surfaces through flow-topography interactions, as well as smaller-scale stirring by mesoscale and submesoscale motions. There is increasing evidence from both observational and numerical studies that motions occurring in the mesoscale and submesoscale range are tightly coupled. Mesoscale strain, through the process of frontogenesis, is responsible for the generation of near-surface lateral density gradients that are precursors for strong vertical submesoscale velocities (Archer et al., 2020; Su et al., 2020). A possible scenario is that these enhanced submesoscale velocities in high-EKE regions rapidly inject surface properties to depths of 300 m or even deeper. Llort et al. (2018) did indeed find evidence of deep, unmodified waters (anomalously low AOU values), which only occurred in high-EKE standing meander regions. Yet, these deep anomalies were found in <1% of all float profiles. An alternate scenario, in line with Balwada et al. (2018), Balwada et al. (2021), and Freilich and Mahadevan (2021), and one that is more consistent with the observed ΔAOU values, is that submesoscale motions play the essential role of efficiently carrying surface properties across the base of the mixed layer. After this, stirring along isopycnals, by the same eddies that create the surface density gradients, enhances the transfer of these surface properties to depth. Thus, while attributing ventilation to different physical processes is important for ensuring that they are represented accurately in climate models, the coupling of motions across scales likely makes this task challenging. Accordingly, numerical models that do not fully resolve mesoscale and submesoscale processes may misrepresent the formation of intermediate waters, as well as the concentration of oxygen in the thermocline.

While this study has focused on ventilation pathways of oxygen in the ACC, these results likely have important implications for the spatial variability of air–sea CO_2 fluxes. Oxygen has an equilibrium timescale that is at least an order of magnitude shorter than that of CO_2, which has an equilibration timescale of O(6 months). Combining this study with evidence that ACC standing meanders are also sites of enhanced upwelling (Brady et al., 2021; Tamsitt et al., 2017) suggests that recently ventilated deep waters in these regions may have short surface residence times, and therefore full equilibration with atmospheric CO_2 may not be reached (Jones et al., 2014). This provides further motivation for exploring how localized high-EKE regions impact exchange of waters between the surface and interior and the larger Southern Ocean carbon cycle.

Various estimates of air–sea exchange of CO_2 in the Southern Ocean have identified interannual to decadal-scale variations in the region's ability to provide an atmospheric carbon sink (Gruber et al., 2019; Landschützer et al., 2015). Notably, these estimates are obtained after some form of interpolation or mapping, for example, neural network (Landschützer et al., 2016), of CO_2 measurements from repeat shiptracks that typically do not sample the strongest and most variable EKE regions. Decadal-scale variations in the Southern Ocean carbon sink have been largely attributed to large-scale processes, such as a change in the Southern Annular Mode (Le Quéré et al., 2007; Lovenduski et al., 2008), a southward shift and strengthening of the westerly winds (DeVries et al., 2017), and enhanced stratification due to increased northward advection of sea ice and southward advection of warmer waters (Landschützer et al., 2015). Localized processes may shape the temporal evolution of air–sea fluxes across the Southern Ocean. For instance, Zhang et al. (2021) illustrate that the standing meander associated with the Campbell Plateau governs trends in EKE over the full Pacific basin. This may also extend to air–sea flux properties; for example, Langlais et al. (2017) show that standing meanders dominate the transfer

of anthropogenic carbon to AAIW. This sequestration is underresolved in models and underobserved in situ. Processes at the standing meander level, including enhanced localized winds and jet-submesoscale interactions, may play a vital role in shaping air–sea exchange of climatologically important properties such as CO_2 (Bachman & Klocker, 2020). This aligns with our findings that standing meanders are likely hotspots for ventilation and suggests that dynamics occurring at scales currently unresolved by most climate models are critical for the transfer of atmospheric anomalies to the ocean interior.

5. Conclusions

We provide observational evidence of heterogeneous subsurface vertical distribution of AOU along the full path of the ACC. In both depth and density space, we find substantial differences in AOU linked to enhanced ventilation in high-EKE regions associated with the ACC's major standing meanders. While shifts in the ACC's density surfaces due to topographic steering at standing meanders explain some of the observed distribution, we also identify mechanisms on the submesoscale–mesoscale spectrum that can contribute to the ventilation of AOU. Data from BGC-Argo floats, especially those deployed by the SOCCOM project, have enhanced our ability to understand the processes impacting ventilation across the entire Southern Ocean, and here we use those data to suggest that localized regions of high EKE play an outsized role in such ventilation. Accordingly, it is vital to consider sub-basin-scale variability and, in particular, how temporal variations in high-EKE standing meanders can impact global Southern Ocean properties that influence and reflect biogeochemical cycling.

Data Availability Statement

The float data were collected and made freely available by the International Argo Program and the national programs that contribute to it (https://argo.ucsd.edu, https://www.ocean-ops.org). The Argo Program is part of the Global Ocean Observing System. The float profiles used in this manuscript are available in the Argo Global Data Assembly Center 10 June 2021 screenshot (https://doi.org/10.17882/42182%2385023). Sea level anomaly products were produced and distributed by the Copernicus Marine 360 and Environment Monitoring Service and are available at https://resources.marine.copernicus.eu/product-detail/SEALEVEL_GLO_PHY_L4_MY_008_047/INFORMATION. Finite-size Lyapunov Exponents were produced and distributed by AVISO+ and are available at https://www.aviso.altimetry.fr/en/data/products/value-added-products/fsle-finite-size-lyapunov-exponents.html.

Acknowledgments
L. A. Dove and A. F. Thompson acknowledge funding from National Science Foundation (NSF) award OCE-1756956, the David and Lucille Packard Foundation, and the Resnick Sustainability Institute. L. A. Dove was additionally supported by an NSF Graduate Research Fellowship. D. Balwada and A. R. Gray were supported by NSF Award OCE-1756882. A. R. Gray acknowledges additional funding through National Oceanic and Atmospheric Administration Award NA20OAR4320271 and through NSF's Southern Ocean Carbon and Climate Observations and Modeling Project under Awards PLR-1425989 and OPP-1936222. The authors are grateful for the comments of three anonymous reviewers, which led to the improvement of this manuscript.

References

Abernathey, R. P., & Marshall, J. (2013). Global surface eddy diffusivities derived from satellite altimetry. *Journal of Geophysical Research: Oceans*, *118*(2), 901–916. https://doi.org/10.1002/jgrc.20066

Adams, K. A., Hosegood, P., Taylor, J. R., Sallée, J.-B., Bachman, S., Torres, R., & Stamper, M. (2017). Frontal circulation and submesoscale variability during the formation of a Southern Ocean mesoscale eddy. *Journal of Physical Oceanography*, *47*(7), 1737–1753. https://doi.org/10.1175/JPO-D-16-0266.1

Archer, M., Schaeffer, A., Keating, S., Roughan, M., Holmes, R., & Siegelman, L. (2020). Observations of submesoscale variability and frontal subduction within the mesoscale eddy field of the Tasman Sea. *Journal of Physical Oceanography*, *50*(5), 1509–1529. https://doi.org/10.1175/JPO-D-19-0131.1

Bachman, S. D., & Klocker, A. (2020). Interaction of jets and submesoscale dynamics leads to rapid ocean ventilation. *Journal of Physical Oceanography*, *50*(10), 2873–2883. https://doi.org/10.1175/JPO-D-20-0117.1

Balwada, D., LaCasce, J. H., Speer, K. G., & Ferrari, R. (2020). Relative dispersion in the Antarctic Circumpolar Current. *Journal of Physical Oceanography*, *51*(2), 553–574. https://doi.org/10.1175/JPO-D-19-0243.1

Balwada, D., Smith, K. S., & Abernathey, R. (2018). Submesoscale vertical velocities enhance tracer subduction in an idealized Antarctic Circumpolar Current. *Geophysical Research Letters*, *45*(18), 9790–9802. https://doi.org/10.1029/2018GL079244

Balwada, D., Xiao, Q., Smith, S., Abernathey, R., & Gray, A. (2021). Vertical fluxes conditioned on vorticity and strain reveal submesoscale ventilation.

Barthel, A., Hogg, A. M., Waterman, S., & Keating, S. (2017). Jet–topography interactions affect energy pathways to the deep Southern Ocean. *Journal of Physical Oceanography*, *47*(7), 1799–1816. https://doi.org/10.1175/JPO-D-16-0220.1

Bischoff, T., & Thompson, A. F. (2014). Configuration of a Southern Ocean storm track. *Journal of Physical Oceanography*, *44*(12), 3072–3078. https://doi.org/10.1175/JPO-D-14-0062.1

Brady, R. X., Maltrud, M. E., Wolfram, P. J., Drake, H. F., & Lovenduski, N. S. (2021). The influence of ocean topography on the upwelling of carbon in the Southern Ocean. *Geophysical Research Letters*, *48*(19). https://doi.org/10.1029/2021GL095088

Bushinsky, S. M., Gray, A. R., Johnson, K. S., & Sarmiento, J. L. (2017). Oxygen in the Southern Ocean from Argo floats: Determination of processes driving air-sea fluxes. *Journal of Geophysical Research: Oceans*, *122*(11), 8661–8682. https://doi.org/10.1002/2017jc012923

Chapman, C. C., Hogg, A. M., Kiss, A. E., & Rintoul, S. R. (2015). The dynamics of Southern Ocean storm tracks. *Journal of Physical Oceanography*, *45*(3), 884–903. https://doi.org/10.1175/JPO-D-14-0075.1

Claustre, H., Johnson, K. S., & Takeshita, Y. (2020). Observing the global ocean with biogeochemical-Argo. *Annual Review of Marine Science*, *12*(1), 23–48. https://doi.org/10.1146/annurev-marine-010419-010956

de Boyer Montégut, C., Madec, G., Fischer, A. S., Lazar, A., & Iudicone, D. (2004). Mixed layer depth over the global ocean: An examination of profile data and a profile-based climatology. *Journal of Geophysical Research*, *109*(C12), C12003. https://doi.org/10.1029/2004JC002378

DeVries, T., Holzer, M., & Primeau, F. (2017). Recent increase in oceanic carbon uptake driven by weaker upper-ocean overturning. *Nature*, *542*(7640), 215–218. https://doi.org/10.1038/nature21068

Dove, L. A., Thompson, A. F., Balwada, D., & Gray, A. R. (2021). Observational evidence of ventilation hotspots in the Southern Ocean. *Journal of Geophysical Research: Oceans*, *126*(7), e2021JC017178. https://doi.org/10.1029/2021JC017178

d'Ovidio, F., Fernández, V., Hernández-García, E., & López, C. (2004). Mixing structures in the Mediterranean Sea from finite-size Lyapunov exponents. *Geophysical Research Letters*, *31*(17), L17203. https://doi.org/10.1029/2004GL020328

d'Ovidio, F., Monte, S. D., Alvain, S., Dandonneau, Y., & Lévy, M. (2010). Fluid dynamical niches of phytoplankton types. *Proceedings of the National Academy of Sciences*, *107*(43), 18366–18370. https://doi.org/10.1073/pnas.1004620107

Freilich, M., & Mahadevan, A. (2021). Coherent pathways for subduction from the surface mixed layer at ocean fronts. *Journal of Geophysical Research: Oceans*, *126*(5), e2020JC017042. https://doi.org/10.1029/2020JC017042

Gille, S. T., & Kelly, K. A. (1996). Scales of spatial and temporal variability in the Southern Ocean. *Journal of Geophysical Research*, *101*(C4), 8759–8773. https://doi.org/10.1029/96JC00203

Gray, A. R., Johnson, K. S., Bushinsky, S. M., Riser, S. C., Russell, J. L., Talley, L. D., et al. (2018). Autonomous biogeochemical floats detect significant carbon dioxide outgassing in the high-latitude Southern Ocean. *Geophysical Research Letters*, *45*(17), 9049–9057. https://doi.org/10.1029/2018GL078013

Gruber, N., Landschützer, P., & Lovenduski, N. S. (2019). The variable Southern Ocean carbon sink. *Annual Review of Marine Science*, *11*(1), 159–186. https://doi.org/10.1146/annurev-marine-121916-063407

Hennon, T. D., Riser, S. C., & Mecking, S. (2016). Profiling float-based observations of net respiration beneath the mixed layer. *Global Biogeochemical Cycles*, *30*(6), 920–932. https://doi.org/10.1002/2016GB005380

Ito, T., Follows, M. J., & Boyle, E. A. (2004). Is AOU a good measure of respiration in the oceans? *Geophysical Research Letters*, *31*(17), L17305. https://doi.org/10.1029/2004GL020900

Johnson, K. S., Plant, J. N., Coletti, L. J., Jannasch, H. W., Sakamoto, C. M., Riser, S. C., et al. (2017). Biogeochemical sensor performance in the SOCCOM profiling float array. *Journal of Geophysical Research: Oceans*, *122*(8), 6416–6436. https://doi.org/10.1002/2017JC012838

Jones, D. C., Ito, T., Takano, Y., & Hsu, W.-C. (2014). Spatial and seasonal variability of the air-sea equilibration timescale of carbon dioxide. *Global Biogeochemical Cycles*, *28*(11), 1163–1178. https://doi.org/10.1002/2014GB004813

Kim, Y. S., & Orsi, A. H. (2014). On the variability of Antarctic Circumpolar Current fronts inferred from 1992–2011 altimetry. *Journal of Physical Oceanography*, *44*(12), 3054–3071. https://doi.org/10.1175/JPO-D-13-0217.1

Klein, P., & Lapeyre, G. (2009). The oceanic vertical pump induced by mesoscale and submesoscale turbulence. *Annual Review of Marine Science*, *1*(1), 351–375. https://doi.org/10.1146/annurev.marine.010908.163704

Klocker, A. (2018). Opening the window to the Southern Ocean: The role of jet dynamics. *Science Advances*, *4*(10), eaao4719. https://doi.org/10.1126/sciadv.aao4719

Landschützer, P., Gruber, N., & Bakker, D. C. E. (2016). Decadal variations and trends of the global ocean carbon sink. *Global Biogeochemical Cycles*, *30*(10), 1396–1417. https://doi.org/10.1002/2015GB005359

Landschützer, P., Gruber, N., Haumann, F. A., Rödenbeck, C., Bakker, D. C. E., Van Heuven, S., et al. (2015). The reinvigoration of the Southern Ocean carbon sink. *Science*, *349*(6253), 1221–1224. https://doi.org/10.1126/science.aab2620

Langlais, C. E., Lenton, A., Matear, R., Monselesan, D., Legresy, B., Cougnon, E., & Rintoul, S. (2017). Stationary Rossby waves dominate subduction of anthropogenic carbon in the Southern Ocean. *Scientific Reports*, *7*(1), 17076. https://doi.org/10.1038/s41598-017-17292-3

Le Quéré, C., Rödenbeck, C., Buitenhuis, E. T., Conway, T. J., Langenfelds, R., Gomez, A., et al. (2007). Saturation of the Southern Ocean CO_2 sink due to recent climate change. *Science*, *316*(5832), 1735–1738. https://doi.org/10.1126/science.1136188

Lévy, M., Franks, P. J. S., & Smith, K. S. (2018). The role of submesoscale currents in structuring marine ecosystems. *Nature Communications*, *9*(1), 4758. https://doi.org/10.1038/s41467-018-07059-3

Llort, J., Langlais, C., Matear, R., Moreau, S., Lenton, A., & Strutton, P. G. (2018). Evaluating Southern Ocean carbon eddy-pump from biogeochemical-Argo floats. *Journal of Geophysical Research: Oceans*, *123*(2), 971–984. https://doi.org/10.1002/2017JC012861

Lovenduski, N. S., Gruber, N., & Doney, S. C. (2008). Toward a mechanistic understanding of the decadal trends in the Southern Ocean carbon sink. *Global Biogeochemical Cycles*, *22*(3), GB3016. https://doi.org/10.1029/2007GB003139

Mahadevan, A. (2016). The impact of submesoscale physics on primary productivity of plankton. *Annual Review of Marine Science*, *8*(1), 161–184. https://doi.org/10.1146/annurev-marine-010814-015912

McDougall, T. J., & Barker, P. M. (2011). Getting started with TEOS-10 and the Gibbs Seawater (GSW) oceanographic toolbox. *Scor/iapso WG*, *127*, 1–28.

Morrison, A. K., Waugh, D. W., Hogg, A. M., Jones, D. C., & Abernathey, R. P. (2022). Ventilation of the Southern Ocean pycnocline. *Annual Review of Marine Science*, *14*(1), 405–430. https://doi.org/10.1146/annurev-marine-010419-011012

Naveira Garabato, A. C., Ferrari, R., & Polzin, K. L. (2011). Eddy stirring in the Southern Ocean. *Journal of Geophysical Research*, *116*(C9), C09019. https://doi.org/10.1029/2010JC006818

Rintoul, S. R. (2018). The global influence of localized dynamics in the Southern Ocean. *Nature*, *558*(7709), 209–218. https://doi.org/10.1038/s41586-018-0182-3

Riser, S. C., Freeland, H. J., Roemmich, D., Wijffels, S., Troisi, A., Belbéoch, M., et al. (2016). Fifteen years of ocean observations with the global Argo array. *Nature Climate Change*, *6*(2), 145–153. https://doi.org/10.1038/nclimate2872

Roach, C. J., Balwada, D., & Speer, K. (2016). Horizontal mixing in the Southern Ocean from Argo float trajectories. *Journal of Geophysical Research: Oceans*, *121*(8), 5570–5586. https://doi.org/10.1002/2015JC011440

Roach, C. J., Balwada, D., & Speer, K. (2018). Global observations of horizontal mixing from Argo float and surface drifter trajectories. *Journal of Geophysical Research: Oceans*, *123*(7), 4560–4575. https://doi.org/10.1029/2018jc013750

Roemmich, D., Johnson, G. C., Riser, S., Davis, R., Gilson, J., Owens, W. B., et al. (2009). The Argo Program: Observing the global ocean with profiling floats. *Oceanography*, *22*(2), 34–43. https://doi.org/10.5670/oceanog.2009.36

Rosso, I., Hogg, A. M., Kiss, A. E., & Gayen, B. (2015). Topographic influence on submesoscale dynamics in the Southern Ocean. *Geophysical Research Letters*, *42*(4), 1139–1147. https://doi.org/10.1002/2014GL062720

Sallée, J.-B., Matear, R. J., Rintoul, S. R., & Lenton, A. (2012). Localized subduction of anthropogenic carbon dioxide in the Southern Hemisphere oceans. *Nature Geoscience*, *5*(8), 579–584. https://doi.org/10.1038/ngeo1523

Siegelman, L., Klein, P., Rivière, P., Thompson, A. F., Torres, H. S., Flexas, M., & Menemenlis, D. (2020). Enhanced upward heat transport at deep submesoscale ocean fronts. *Nature Geoscience*, *13*(1), 50–55. https://doi.org/10.1038/s41561-019-0489-1

Sokolov, S., & Rintoul, S. R. (2007). Multiple jets of the Antarctic Circumpolar Current south of Australia. *Journal of Physical Oceanography*, *37*(5), 1394–1412. https://doi.org/10.1175/JPO3111.1

Su, Z., Torres, H., Klein, P., Thompson, A. F., Siegelman, L., Wang, J., et al. (2020). High-frequency submesoscale motions enhance the upward vertical heat transport in the global ocean. *Journal of Geophysical Research: Oceans*, *125*(9), e2020JC016544. https://doi.org/10.1029/2020JC016544

Tamsitt, V., Drake, H. F., Morrison, A. K., Talley, L. D., Dufour, C. O., Gray, A. R., et al. (2017). Spiraling pathways of global deep waters to the surface of the Southern Ocean. *Nature Communications*, *8*(1), 1–10. https://doi.org/10.1038/s41467-017-00197-0

Tamsitt, V., Talley, L. D., Mazloff, M. R., & Cerovečki, I. (2016). Zonal variations in the Southern Ocean heat budget. *Journal of Climate*, *29*(18), 6563–6579. https://doi.org/10.1175/JCLI-D-15-0630.1

Thompson, A. F., & Naveira Garabato, A. C. (2014). Equilibration of the Antarctic Circumpolar Current by standing meanders. *Journal of Physical Oceanography*, *44*(7), 1811–1828. https://doi.org/10.1175/JPO-D-13-0163.1

Uchida, T., Balwada, D., Abernathey, R. P., McKinley, G. A., Smith, S. K., & Lévy, M. (2020). Vertical eddy iron fluxes support primary production in the open Southern Ocean. *Nature Communications*, *11*(1), 1125. https://doi.org/10.1038/s41467-020-14955-0

Viglione, G. A., & Thompson, A. F. (2016). Lagrangian pathways of upwelling in the Southern Ocean. *Journal of Geophysical Research: Oceans*, *121*(8), 6295–6309. https://doi.org/10.1002/2016JC011773

Villermaux, E. (2019). Mixing versus stirring. *Annual Review of Fluid Mechanics*, *51*(1), 245–273. https://doi.org/10.1146/annurev-fluid-010518-040306

Youngs, M. K., Thompson, A. F., Lazar, A., & Richards, K. J. (2017). ACC meanders, energy transfer, and mixed barotropic–baroclinic instability. *Journal of Physical Oceanography*, *47*(6), 1291–1305. https://doi.org/10.1175/JPO-D-16-0160.1

Zhang, Y., Chambers, D., & Liang, X. (2021). Regional trends in Southern Ocean eddy kinetic energy. *Journal of Geophysical Research: Oceans*, *126*(6), e2020JC016973. https://doi.org/10.1029/2020JC016973